

Design of a wavelength frame multiplication system using acceptance diagrams

D. Nekrassov^{a,b,*}, C. Zendler^{a,b}, K. Lieutenant^{a,b}

^a*Helmholtz-Zentrum Berlin, Hahn-Meitner-Platz 1, D-14109 Berlin, Germany*

^b*German Work Package for the ESS Design Update*

Abstract

The concept of Wavelength Frame Multiplication (WFM) was developed to extend the usable wavelength range on long pulse neutron sources for instruments using pulse shaping choppers. For some instruments, it is combined with a pulse shaping double chopper, which defines a constant wavelength resolution, and a set of frame overlap choppers that prevent spurious neutrons from reaching the detector thus avoiding systematic errors in the calculation of wavelength from time of flight. Due to its complexity, the design of such a system is challenging and there are several criteria that need to be accounted for. In this work, the design of the WFM chopper system for the potential future liquids reflectometer at the European Spallation Source (ESS) is presented, which makes use of acceptance diagrams. They prove to be a powerful tool for understanding the work principle of the system and recognizing potential problems. The authors assume that the presented study can be useful for design or upgrade of further instruments, in particular the ones planned for the ESS.

1. Introduction

There is currently an increasing demand for neutron instruments, at which the resolution can be adjusted, in particular towards high-resolution setups. The total instrument resolution in neutron scattering experiments always depends, amongst others, on the experimental $\delta\lambda/\lambda$ resolution, where λ is the neutron wavelength. In time-of-flight (ToF) mode, the experimental resolution is determined by pulse shaping choppers for all instruments at continuous sources and for high or medium resolution on long pulse sources. A particular system of rotating disc choppers provides the desired waveband and removes contaminant neutrons. For some experiments like small-angle neutron scattering or neutron reflectometry, it is often desirable to have a constant wavelength resolution over the entire usable waveband. For reactor sources, this can be achieved by introducing a pulse shaping double chopper operating in optically blind mode [1]. In this case, the wavelength resolution is determined by the ratio of the distance D between the pulse shaping choppers and the distance L_0 between the center of the double chopper system and the detector: $\delta\lambda/\lambda = D/L_0$. This relation is

*Corresponding author

Preprint submitted to *EPJ Special Topics* on August 13, 2018
 dmitry.nekrassov@helmholtz-berlin.de (D. Nekrassov),
 carolin.zendler@helmholtz-berlin.de (C. Zendler),
 klaus.lieutenant@helmholtz-berlin.de (K. Lieutenant)

37 valid for all wavelengths up to $\lambda = \frac{3956}{D/\tau}[\text{\AA}]$, where τ is the single disc opening
38 time.

39
40 At pulsed sources, like the currently planned European Spallation Source
41 (ESS) [2], the chopper design described above [1] is usually not applicable in
42 its simple form. The reason is that due to the needed shielding volume, the
43 first chopper can be placed only at a certain minimum distance away from the
44 source, which is currently 6 m for the ESS. Depending on the desired wave-
45 band, this implicates that not all neutrons will be at the first chopper at the
46 same time, which limits the usable waveband at the detector. To extend this
47 range, the WFM concept was developed [3]. It was then complemented with
48 a blind double-chopper setup to create a wavelength dependent pulse length
49 [4]. Here, the combination with a blind double-chopper setup is used to obtain
50 a constant wavelength resolution. To achieve a sufficiently broadband pulse
51 within the main frame (given by the pulse repetition rate), this concept utilizes
52 multiple subframes. These subframes are constructed such that the wavelength
53 resolution is the same for every subframe and they are separated in time at the
54 detector, but at the same time the measurement time is efficiently used, i.e. the
55 time gaps between individual subframes are minimised. The proof of principle
56 of the WFM approach was achieved at the Budapest Neutron Center (BNC) [5].

57
58 At the future ESS, several instruments will need to implement the WFM
59 approach. The chopper layout must be carefully adapted to the long pulse
60 structure of the ESS beam. Neutrons being detected in the wrong subframe
61 can pose a significant source of systematic errors ¹, so in particular the choice
62 of frame overlap chopper parameters must be done with great care. The need
63 for a thorough analysis method was lastly shown by several technical challenges
64 experienced during the conception of a WFM chopper layout using time-of-flight
65 diagrams for the ESS test beamline in Berlin [8]. In this paper, the design of a
66 WFM setup carried out in the context of a design study of a liquids reflectometer
67 to be proposed for the ESS, is demonstrated by using acceptance diagrams based
68 on the work presented in [6].

69 **2. Application of acceptance diagrams for WFM system of the ESS** 70 **liquids reflectometer**

71 *2.1. Designing the pulse shaping choppers*

72 In a WFM chopper setup, the parameters of the pulse shaping choppers
73 (PSCs) have to be calculated first. These depend on the global parameters
74 being the total length L_{tot} of the instrument and the width of the waveband
75 $\Delta\lambda = \lambda_{\text{max}} - \lambda_{\text{min}}$, where λ_{min} and λ_{max} are the minimal and maximal design

¹or spoil some fraction of the dataset and thereby lengthen the measurement time, if a contaminated part of a subframe has to be removed from the later data analysis.

76 wavelengths, respectively. The instrument length and the waveband width are
77 related through the source period T :

$$\Delta\lambda = h/m_n \times T/L_{\text{tot}}, \quad (1)$$

78 where h is Planck's constant and m_n is the neutron mass. In addition, it
79 is important to decide on the loosest wavelength resolution $R_{\text{max}} = (\delta\lambda/\lambda)_{\text{max}}$
80 in the WFM regime. Once these parameters are given, then the distance $D =$
81 $L_0 \times (\delta\lambda/\lambda)_{\text{max}}$ between the two choppers, the number of windows, their sizes
82 and offsets with respect to each other can be calculated (see Fig. 1). The
83 windows of the PSCs are designed such that they enable measurements with
84 the loosest design resolution R_{max} , with the distance between the two choppers
85 being

$$D = L_2 - L_1 = L_0 \times R_{\text{max}}, \quad (2)$$

86 where L_1 (L_2) is the position of the first (second) PSC chopper. Higher reso-
87 lutions are then achieved by reducing the distance between the two choppers [1].
88

89 The design of the chopper windows starts by calculating the time $t_{1,1}^C$ when
90 the first window ($W_{1,1}$) of the first chopper Ch_1 closes. This time is set by
91 neutrons of wavelength λ_{min} starting at the end of the pulse, see Fig. 1:

$$t_{1,1}^C = L_1/v(\lambda_{\text{min}}) + t_0 \quad (3)$$

92 The PSCs operate in the optical blind mode, i.e. the second chopper opens
93 when the first one closes. Thus $t_{2,1}^O = t_{1,1}^C$. The opening time $t_{1,1}^O$ of the window
94 $W_{1,1}$ is then given by the slowest neutrons that can reach the second chopper
95 when the window $W_{2,1}$ opens, which start at the source at the beginning of the
96 pulse or after some offset δt_0 :

$$t_{1,1}^O = \frac{L_1}{\check{v}_1} + \delta t_0, \quad (4)$$

97 where $\check{v}_1 = L_2/(t_{2,1}^O - \delta t_0)$. The closing time $t_{2,1}^C$ of the window $W_{2,1}$ is given
98 by the slowest neutrons with the wavelength $\lambda_{\text{max},1}$ that reach the first chopper
99 when it closes:

$$t_{2,1}^C = \frac{L_2}{v_{\text{min},1}} + \delta t_0, \quad (5)$$

100 where $v_{\text{min},1} = L_1/(t_{1,1}^C - \delta t_0)$. Note that λ_{min} is not the shortest wavelength
101 that gets transmitted through the PSC (see Fig. 1), but is the shortest wave-
102 length for which the created pulse length δt corresponds to the resolution R_{max} .
103 At the same time, if $\delta t_0 > 0$, then $\lambda_{\text{max},1} = \lambda(v_{\text{min},1})$ is also not the largest
104 wavelength that gets transmitted through the first window of the PSCs. For
105 the design of the second window, the shortest wavelength is set $\lambda_{\text{min},2} = \lambda_{\text{max},1}$
106 to achieve a continuous spectrum and minimise time gaps at the detector, and

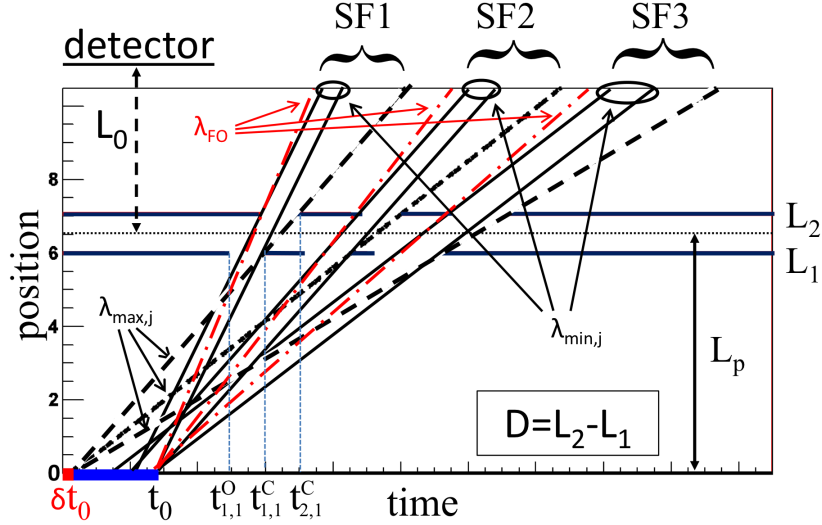


Figure 1: Illustration of the construction procedure of the PSC with a ToF diagram. The total pulse duration t_0 is denoted by the blue bar, while the time offset δt_0 is illustrated by the red square, thus the usable pulse length is $t_0 - \delta t_0$. The choppers are located at the positions L_1 and L_2 . For the j th subframe SF, neutrons having the wavelength $\lambda_{\min,j}$ and $\lambda_{\max,j}$ used in Eqs. 3 and 5 are shown by black lines. Neutrons with wavelengths $\lambda_{\text{FO}} < \lambda_{\min,j}$ responsible for potential subframe overlap, are depicted by dashed-dotted red lines. In addition, the chopper system parameters D being the distance between both PSCs, the distance between the source and the centre of the PSC system L_p and L_0 , which is the distance between the centre of the PSC system and the detector that is well outside the illustrated region, are also shown. See text for further details.

107 the construction procedure is repeated iteratively. Thus neutrons with wave-
 108 lengths $\lambda < \lambda_{\min,j}$ or $\lambda > \lambda_{\max,j}$ that get transmitted through the j th window
 109 of the PSCs can lead to overlap of the subframes in time at some distance be-
 110 hind the PSCs and must be treated by frame overlap choppers. Their design is
 111 discussed in the next subsection.

112

113 A PSC constructed in the way described above transmits a certain fraction
 114 of the total available phase space. The latter is obtained by performing a fixed
 115 grid scan through the $[t, \lambda]$ parameter space assuming a constant spectrum as
 116 a function of the wavelength λ , where t is the start time of a neutron at the
 117 source. This can be visualised in an acceptance diagram (Fig. 2) displaying the
 118 correlation between the neutron wavelength λ and the time t_{PS} , at which the
 119 neutron is at the position $L_p = L_1 + 1/2 \times D$ located in the center between
 120 both PSCs. As an example, instrument parameters calculated for a potential
 121 ESS liquids reflectometer (*instrument I*) (see Table 1) are used in the most of
 122 the following discussion. The initially available phase space is split by the PSCs
 123 into 3 subframes being disjoint in time but joint in wavelength ranging from 2 Å

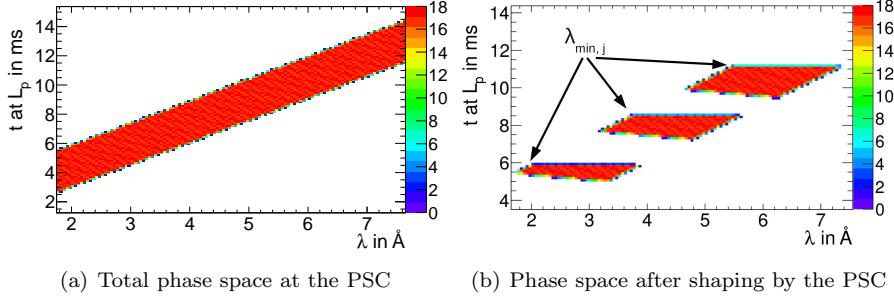


Figure 2: Neutron phase space available at the PSC for the *instrument I*, displayed as correlation between the neutron wavelength λ and the ToF at the position between the PSCs. This phase space has been determined by a fixed grid scan through the $[\lambda, t]$ parameter space. The units on the z-axis are arbitrary and correspond to the phase space density. Without any pulse shaping, the phase space is linearly correlated and has the ESS pulse width of 2.86 ms for each wavelength. After pulse shaping, the phase space is divided into three subframes, with the width $\delta t(\lambda)$ corresponding to the design resolution.

124 to 7.2 Å, based on a instrument length of $L_{\text{tot}} = 55$ m. For each λ , the total
 125 width $\delta t(\lambda)$ of the modified pulse corresponds to the design resolution 2.2% of
 126 the WFM system. If no further choppers would be included in the system, due
 127 to wavelength overlap of individual subframes discussed above, the subframes
 128 would inevitably overlap in time at some distance after the PSC. Thus frame
 129 overlap choppers are needed to keep the subpulses separated until they reach
 130 the detector. Their number and positions are optimised in the following using
 131 acceptance diagrams.

132

133 2.2. Designing the frame overlap choppers

134 Frame overlap choppers (FOCs) can be visualised in the acceptance diagram
 135 as linear functions indicating the opening and closing of the corresponding chop-
 136 per window. Points in the phase space described by these functions correspond
 137 to certain $[t, \lambda]$ combinations such that these neutrons reach the corresponding
 138 chopper at the time when it opens or closes. The analytical description of these
 139 functions for the opening and closing time is:

$$\begin{aligned}
 t_{i,j}^{O/C} = f(\lambda) &= -((L_i - L_P)/v(\lambda)) + \Theta_{i,j}^{O/C}/\omega_i \\
 &= -((L_i - L_P) \times m/h) \times \lambda + \Theta_{i,j}^{O/C}/\omega_i,
 \end{aligned}
 \tag{6}$$

140 where L_i is the distance between the Chopper i and the source, $v(\lambda) = \frac{h}{m\lambda}$
 141 the neutron velocity, $\Theta_{i,j}^{O/C}$ the angular offset of the window start (end) j with
 142 respect to the guide position and ω_i the chopper rotation frequency. At a
 143 pulsed source, chopper frequencies have to be equal to the source frequency or

144 larger by an integer factor. Fractional distances between the PSCs² and the
 145 detector act thereby as a limit for maximum possible multiple of the source
 146 frequency, e.g. choppers only can rotate at twice (four times) the source fre-
 147 quency, if their distance D_i to the PSCs fulfills $D_i \leq 1/2L_0$ ($1/4L_0$) and so on.
 148 Thus as a first choice, three FOCs can be placed at $1/8L_0 + L_1 = 12.125$ m,
 149 $1/4L_0 + L_1 = 18.25$ m and $1/2L_0 + L_1 = 30.5$ m. The windows of a FOC i are
 150 then constructed such that they open when they are reached by the fastest neu-
 151 tron starting at $t_j^{\lambda_{\min,j}} = t_{2,j}^O - L_2/v(\lambda_{\min,j})$ and close upon arrival of the slowest
 152 neutron of the corresponding subframe j starting at δt_0 . Based on these fore-
 153 going considerations, the window parameters j of the FOC i can be calculated
 154 in a straightforward way:

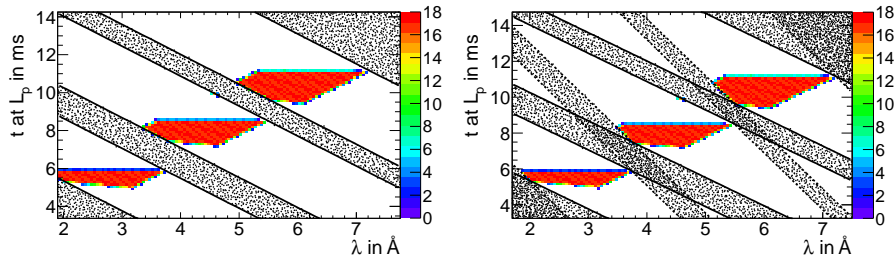
$$\Theta_{i,j}^O = -\omega_i \times \left(\frac{L_i}{v(\lambda_{\min,j})} + t_j^{\lambda_{\min,j}} \right) \quad (7)$$

$$\Theta_{i,j}^C = -\omega_i \times \left(\frac{L_i}{v(\lambda_{\max,j})} + \delta t_0 \right) \quad (8)$$

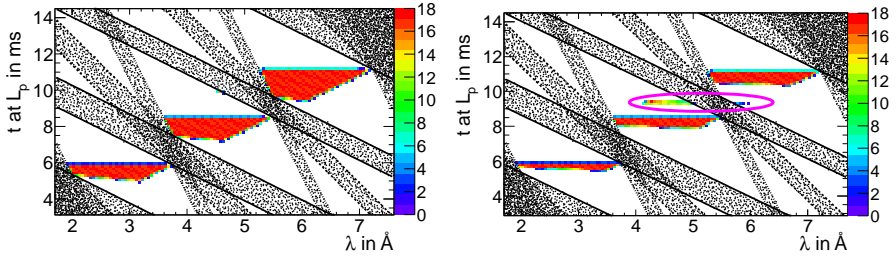
155 The inclusion of FOCs restricts parts of the phase space transmitted through
 156 the PSCs (Fig. 3). This leads to a reduced transmission for wavelengths be-
 157 ing in the overlap region of the individual subframes. The level of such a flux
 158 reduction also depends on other instrument parameters and is discussed in the
 159 next section, while this discussion is more focused on whether the FOCs keep
 160 all the unwanted phase space away from the subframes. While it appears that
 161 for the loosest resolution of $\delta\lambda/\lambda = 2.2\%$ the transmitted parameter space is in
 162 accordance with expectations, at a higher resolution of 1%, when the discs of
 163 the PSCs are closer together, there is a leakage of phase space into subframes
 164 2 and 3, which spoils the desired resolution. Thus the previously chosen layout
 165 of FOCs does not work properly for all adjustable WFM settings.

166
 167 The position of the contaminant phase space in the diagram suggests that
 168 an additional FOC located very close to the PSC, i.e. represented by lines with
 169 a very small slope, would be able to remove the frame overlap while at the
 170 same time not cut into the usable phase space. This is confirmed in Fig. 4,
 171 showing the addition of a FOC at 7.5 m, while also the positions of other three
 172 FOCs were slightly changed (see Tab. 1 and Fig. 6). Contaminant radiation is
 173 now removed even for high resolutions while saving as much as possible of the
 174 usable phase space. In Fig. 5, analytical calculations of neutron propagation
 175 through this chopper setup show that all subframes are separated in time at the
 176 detector position, while the adjusted resolution is achieved for a greater part
 177 of the usable waveband. For wavelengths close to a neighbouring (sub)frame,
 178 the resolution and thus the transmission is reduced due to prevention of frame
 179 overlap. As the next step, the validity of this layout needs to be confirmed by

²or the source if the pulse is not shaped afterwards.

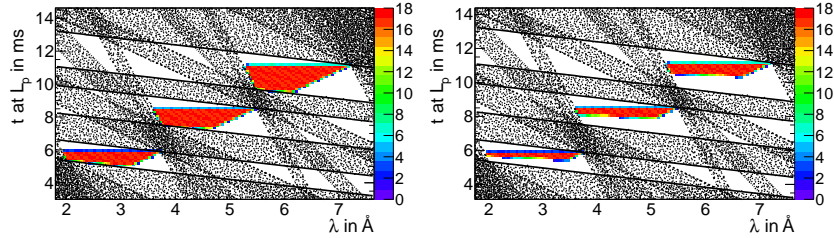


(a) Phase space after inclusion of FOC1 at 12.125 m (b) Phase space after inclusion of FOC2 at 18.25 m



(c) Phase space after inclusion of FOC3 at 30.5 m (d) Phase space for 1% resolution

Figure 3: Remaining phase space after subsequent inclusion of frame overlap choppers at 12.125 m, 18.25 m and 30.5 m. Areas that are excluded by the FOCs are shaded. While there is hardly any contaminant radiation left for the design resolution of 2.2%, there is a clear leakage of spurious neutrons highlighted by the magenta ellipse into the second and third subframe when reducing the distance between the two discs of the PSC to achieve a resolution of 1%.



(a) Phase space after all choppers for 2.2% resolution. (b) Phase space after all choppers for 1% resolution.

Figure 4: The inclusion of a fourth FOC at 7.5 m removes the contaminant radiation present in the WFM setup shown in Fig. 3. Now even for resolutions of 1% (and higher) the transmitted phase space is free of spurious neutrons.

180 neutronic Monte-Carlo (MC) simulations, described in the following section.

181

182 3. Comparison with MC simulations

183 The analytical study described in the last section makes use of idealised
 184 conditions. In a real instrument, the characteristics of the transmitted neutron
 185 beam will be influenced by additional parameters like guide geometry, beam di-
 186 vergence and pulse structure, and chopper rotation speed. Thus to confirm that
 187 the WFM chopper layout derived from analytical considerations is suitable for
 188 a real instrument, it needs to be tested by a neutron MC simulation, where all
 189 of these criteria are included. In this work, the VITESS software [7, 9] package
 190 was used. The chopper setup was included in the simulations of the *instrument*
 191 *I*, which will be published elsewhere.

192

193 3.1. Simulations of the reflectometer chopper layout

194 In order to include the choppers in the MC simulation, it is important to
 195 decide on their parameters like radius and rotation speed. The radius and rota-
 196 tion speed might be constrained by their position in the particular instrument
 197 and engineering feasibility. It is also important to decide how to deal with the
 198 finite time a chopper needs to fully open or close the beam. First, in order to
 199 be conservative and prevent frame overlap as far as possible, the time $t_{i,j}^O$ ($t_{i,j}^C$),
 200 at which the i th chopper opens (closes) the guide in the analytical calculation,
 201 is defined as the time at which the chopper starts to open (fully closes) the
 202 beam in the simulation, see Fig. 7. This requirement guarantees that for each
 203 wavelength the neutron transmission starts and ends at the same time as in
 204 the phase space study. Hence the size of the windows has to be reduced to
 205 account for the time the choppers need to sweep through the guide. As a re-
 206 sult, for a given nominal resolution simulations should yield a higher measured

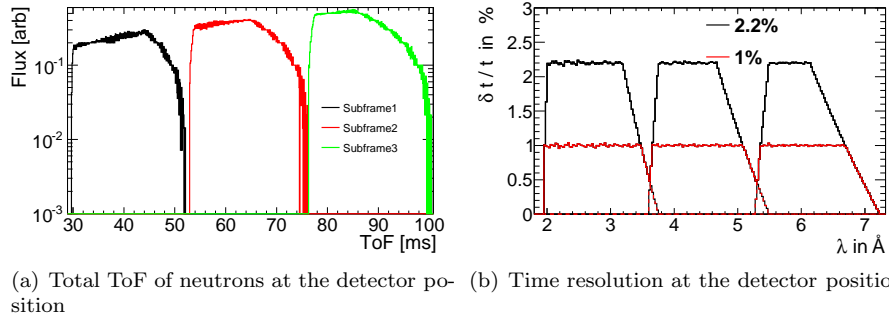


Figure 5: Left: ToF plot of 3 subframes coming from a single main pulse, which are well separated in time. Right: The wavelength resolution at the detector expressed as $\delta t(\lambda)/t_{\text{tot}}(\lambda)$, where t_{tot} is the ToF of neutrons between the centre of the PSC and the detector. The contributions of individual subframes are denoted by dashed lines, whereas the maximum resolution is depicted by the solid lines. Since the subframes are separated in time, it allows for an unambiguous reconstruction of the wavelength from ToF.

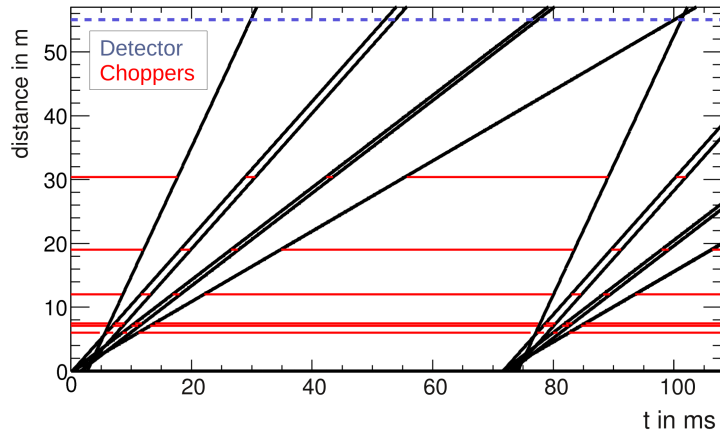


Figure 6: Time of flight diagram of the final chopper setup as worked out with the acceptance diagram method. The fastest and slowest of neutrons trajectories in the individual subframes are represented by black lines, while choppers and the detector are depicted by the red and blue lines, respectively. For completeness, the next main pulse is shown as well.

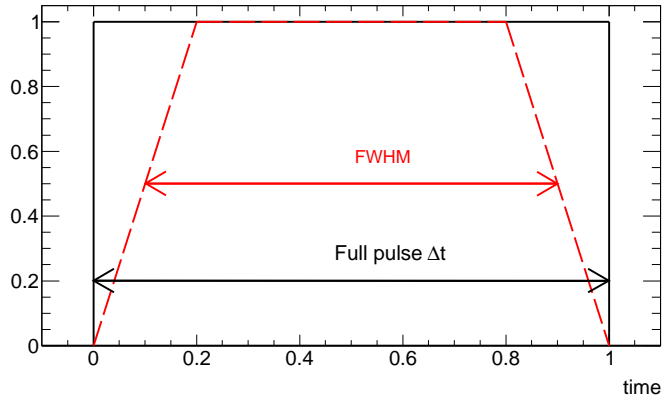


Figure 7: Illustration of the neutron pulse structure used in the analytical study and MC simulations. While in the analytical study the opening and closing time of choppers were assumed to be infinitely small and thus the pulse was a perfect rectangle with a width of $\Delta t(\lambda)$, the finite guide size and chopper rotation speed lead to a trapezoidal shape of the pulse. Its full width at half maximum (FWHM) is smaller than the pulse duration Δt , since in this work the points in time at which pulse starts and ends in the MC simulation were decided to exactly coincide with those from the phase space study.

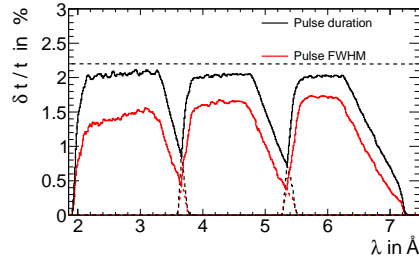
207 resolution at the cost of a reduced transmission due to a smaller FWHM of the
 208 pulse. A deviation from this strict requirement is considered in the next section.

209

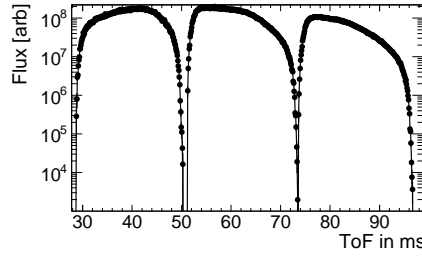
210 To prove that the WFM setup works in the MC simulation, it is important
 211 to show that both the desired resolution is reached and the subframes are well
 212 separated in time. Results of VITESS simulations shown in Fig. 8 confirm that
 213 the subframes are well separated in time and the time gap between subframes
 214 coincides with analytical results. As far as the achieved time resolution is con-
 215 cerned, it can be observed that especially for short wavelengths it is higher than
 216 the nominal resolution, thus the neutron transmission is slightly worse in MC
 217 simulations compared with the transmission from analytical calculations. The
 218 wavelength spectrum exhibits dips as a result of frame overlap prevention, see
 219 Fig. 9 and Fig. 5 and 8 for comparison.

220 3.2. Impact of technical constraints

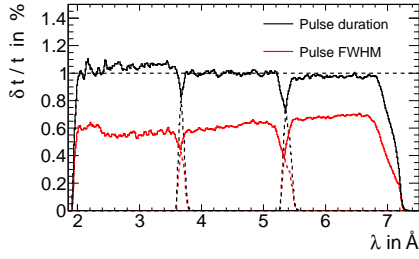
221 In the last section it was shown that the WFM setup as developed with
 222 the help of acceptance diagrams proved to work in the MC simulation of the
 223 *instrument I*. Compared to analytical calculations, geometrical constraints of
 224 the instrument have an impact on the neutron transmission and lead to time
 225 pulses, which deviate from the idealised rectangular shape (see Fig. 7). This
 226 has an effect on the achieved wavelength resolution (Fig. 8) and overall neu-
 227 tron flux (Fig. 9). As far as the resolution is concerned, in order to achieve
 228 the desired value either the distance between the discs of the PSC needs to be



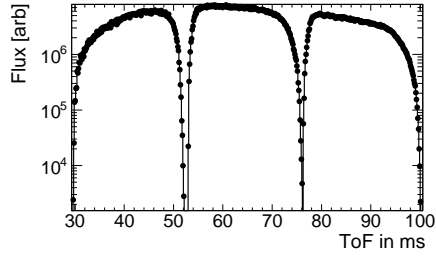
(a) Time resolution at the detector position for 2.2%



(b) Time distribution at the detector position for 2.2%



(c) Time resolution at the detector position for 1%



(d) Time distribution at the detector position for 1%

Figure 8: (a) and (c): Measured time resolution at the detector position as a function of wavelength, which was calculated using both the total pulse duration $t_{\max} - t_{\min}(\lambda)$ and its FWHM (see also Fig. 7). As expected, the total pulse duration agrees well with analytical results while for the FWHM calculation the trapezoidal shape of the pulses due to finite guide geometry and chopper rotation speed comes into play. (b) and (d): ToF distribution at the detector position, all subframes are clearly separated in time by the WFM setup.

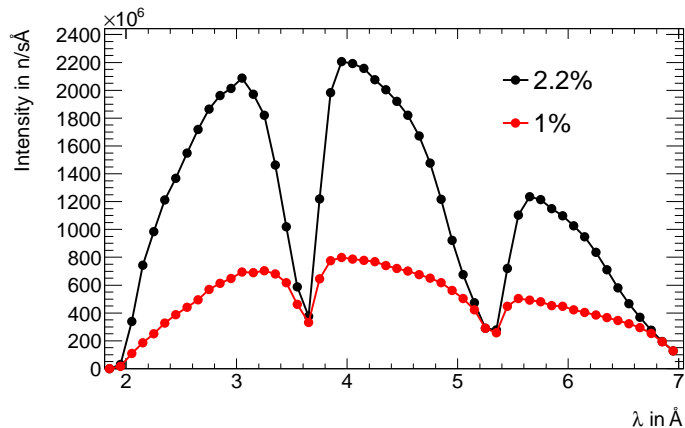
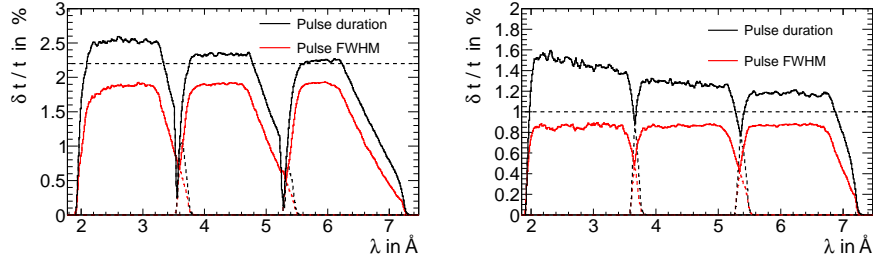


Figure 9: Neutron flux at the detector position for the *instrument I* comprising a WFM chopper layout for 2.2% and 1% wavelength resolution. For wavelengths close to the subframe edges a reduction of flux due to frame overlap prevention can be observed.

229 increased or the windows of the PSC should be modified. The latter can be
 230 done by withdrawing the reduction of the window widths that accounted for
 231 finite guide dimensions, i.e. dropping the strict requirement concerning chopper
 232 opening and closing times by assuming that the beam is infinitely thin. This
 233 leads to an increase of the total pulse width, but at the same time the FWHM
 234 of the pulse, which is the factor determining the wavelength resolution at the
 235 detector, better corresponds to the desired value, see Fig. 10. Such a choice of
 236 window parameters for the PSC can be recommended as a solution to the pulse
 237 shape problem coming from finite instrument dimensions. Flux losses in the
 238 regions around subframe edges, which come from FOCs cutting into the beam
 239 to avoid frame overlap, can be reduced by optimizing the sizes and offsets of
 240 chopper windows such that the time gap between subframes is minimised and
 241 the opening and closing time is reduced (see Fig. 11).

242

243 It should be mentioned that the *instrument I* does not have the most diffi-
 244 cult conditions in terms of the complexity of the WFM system, both in terms
 245 of the used wavelength band and instrument geometry, in particular taking into
 246 account the small height of the neutron guide of 2 cm. To prove that the concept
 247 still works in more challenging conditions as well, it was applied to a compar-
 248 able instrument (*instrument II*) requiring a constant resolution for wavelengths
 249 between 1 Å and about 10 Å and having a guide cross section of $9 \times 9 \text{ cm}^2$
 250 for the most of the length of the instrument. The chopper layout worked out with
 251 acceptance diagrams was very similar to the one for *instrument I*, again com-
 252 prising six choppers and in particular with the first FOC being placed very close
 253 to the PSC, which is again located at 6 m. While the PSC and the first FOC



(a) Measured resolution at the detector position for nominal resolution of 2.2% (b) Measured resolution at the detector position for nominal resolution of 1%

Figure 10: Wavelength resolution measured at the detector position using the total width and FWHM of time pulses as a function of wavelength. The effect of reduced and wavelength dependent FWHM due to finite instrument geometry and chopper speed (see Fig. 8) is corrected by modifying the windows of the PSC. See text for further details.

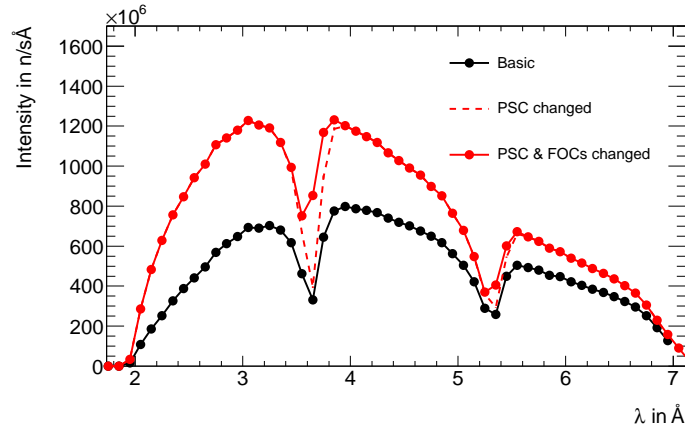
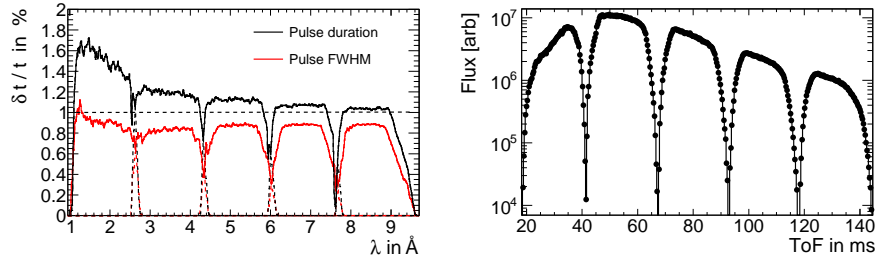


Figure 11: Neutron flux at the detector position for the *instrument I* comprising a WFM chopper layout for 1% wavelength resolution. The basic configuration of choppers, depicted by the black line, was modified to maximize the flux output in the regions where subframes overlap in wavelength. An improved performance was reached when modifying the windows of the PSC as well as those of FOCs.



(a) Measured resolution at the detector position for nominal resolution of 1% (b) Measured ToF at the detector position for nominal resolution of 1%

Figure 12: Measured resolution and ToF distribution for the *instrument II* having a $9 \times 9 \text{ cm}^2$ guide cross section for the most length and utilizing wavelengths between 1 and around 10 \AA . The chopper layout designed with acceptance diagrams allows to reach the adjusted resolution by splitting the waveband into five subframes that do not overlap in time.

254 deal with a focused beam of a $2 \times 2 \text{ cm}^2$ cross section ³, the full guide cross
 255 section of $9 \times 9 \text{ cm}^2$ is seen at the positions of the remaining three FOCs. MC
 256 simulations show that also in this case the chopper system delivers the desired
 257 resolution for the entire waveband, which is split into five subframes being all
 258 separated in time as required (Fig. 12). The flux losses due to frame overlap
 259 avoidance increase, since the larger guide dimensions and smaller chopper speed
 260 due to the increased transmitted waveband require longer opening and closing
 261 chopper times than for the *instrument I*. This situation can be improved by
 262 minimising the time gap between subframes (see Fig. 13). For this, acceptance
 263 diagrams once more prove to help by pointing out the right chopper parameters
 264 for a modification. Compared to the *instrument I*, there is more flux lost in
 265 the overlap regions, however the total flux reduction only amounts to about
 266 20%, if compared to a layout in which FOCs would be excluded. In general, the
 267 spectrum transmitted by a WFM system and its optimisation will be particular
 268 to each instrument, whereas at the same time a chopper layout suggested by
 269 the acceptance diagram approach can be expected to be already close to an
 270 optimum solution.

271 4. Conclusion

272 The WFM concept is a sophisticated chopper setup that enables to expand
 273 the usable wavelength range, in particular in combination with a constant wave-
 274 length resolution setup at long pulse neutron sources. Due to its complexity, the

³If high-resolution measurements are desired, the instrument concept should be such that at the position of the PSC the beam is narrow at least in one dimension. Since at the future ESS there are tight space constraints for choppers placed at around 6 m, a large beam cross section would render pulse shaping for high-resolution mode impossible.

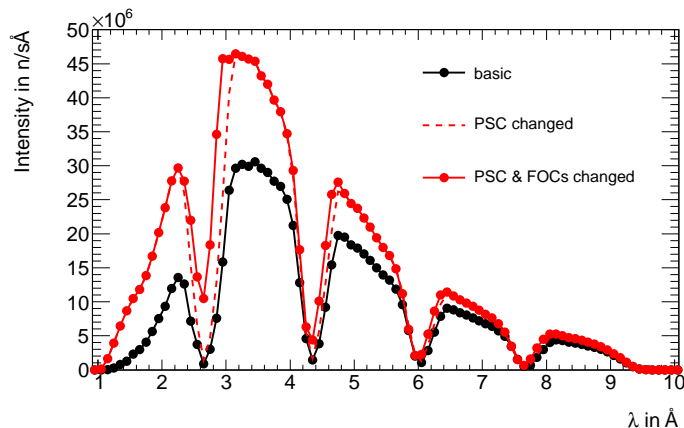


Figure 13: Neutron flux at the detector position for the *instrument II* comprising a WFM chopper layout for 1% wavelength resolution. The basic configuration of choppers, depicted by the black line, was modified to maximize the flux output in the regions where subframes overlap in wavelength. An improved performance was reached when modifying the windows of the PSC as well as those of FOCs. See text for further details.

275 design of such a system is challenging and there are several criteria that need
 276 to be accounted for. As was shown in this work, acceptance diagrams can be a
 277 powerful tool to design and optimise WFM systems, because they help getting
 278 a thorough understanding of the interplay between individual choppers and are
 279 at the same time much faster to process than neutron simulations, thus problems
 280 like contaminant neutrons at higher resolutions would be more difficult
 281 to recognise and solve in MC simulations. Acceptance diagrams allow one to
 282 optimise the number and positions of the WFM choppers such that the beam
 283 characteristics obtained in MC simulations match the instrument requirements
 284 in terms of subframe separation and achieved resolution. The presented WFM
 285 concept works for different instruments independent of their particular geometrical
 286 constraints, thus the acceptance diagram method can be of significant help
 287 when designing or upgrading instruments, in particular in view of the future
 288 ESS facility.

289

290 Acknowledgements

291 We thank M. Trapp, M. Strobl and R. Steitz for their fruitful discussions.
 292 This work was funded by the German BMBF under “Mitwirkung der Zentren
 293 der Helmholtz Gemeinschaft und der Technischen Universität München an der
 294 Design-Update Phase der ESS, Förderkennzeichen 05E10CB1.”

295 **References**

- 296 [1] A. van Well, Physica B 180 (1992) 959-961
- 297 [2] European Spallation Source, URL <http://www.esss.se>
- 298 [3] F. Mezei and M. Russina, Proc. SPIE 4785. Advances in Neutron Scattering
299 Instrumentation (2002) 24-33
- 300 [4] K. Lieutenant and F. Mezei, Journal of Neutron Research (2006) Vol. 14,
301 No. 2, 177-191
- 302 [5] M. Russina et al., Nuclear Instruments and Methods in Physics Research A
303 654 (2011) 383-389
- 304 [6] J. Copley, Nuclear Instruments and Methods in Physics Research A 510
305 (2003) 318-324
- 306 [7] K. Lieutenant et al., Proc. SPIE 5536(1) (2004) 134-145
- 307 [8] M. Strobl and M. Bulat and K. Habicht, Nuclear Instruments and Methods
308 in Physics Research A 705 (2013) 74-84
- 309 [9] Vitess URL <http://www.helmholtz-berlin.de/vitess>

Parameter	Parameter value	
	<i>Instrument I</i>	<i>Instrument II</i>
ESS pulse length t_0	2.86 ms	
ESS source frequency	14 Hz	
Total instrument length L_{tot}	55 m	60 m
Wavelength band	2–7.2 Å	1–9.6 Å
Distance between the PSCs and detector L_0	49 m	54 m
Position of the first PSC	6 m	
Position of the second PSC at 2.2% (1%) resolution	7.08 m (6.49 m)	— (6.54 m)
Rotation frequency of the PSC	70 Hz	
Final position and rotation frequency of the 1st FOC	7.5 m, 70 Hz	7.4 m, 70 Hz
Final position and rotation frequency of the 2nd FOC	12 m, 56 Hz	11.7 m, 42 Hz
Final position and rotation frequency of the 3rd FOC	19 m, 28 Hz	18 m, 28 Hz
Final position and rotation frequency of the 4th FOC	30.4 m, 14 Hz	28 m, 14 Hz
Guide height	2 cm	2 – 9 cm
Guide width	10 – 26 cm	2 – 9 cm

Table 1: Basic preliminary instrument parameters used in the design of the potential future ESS liquids reflectometer (*instrument I*) and for the crosscheck instrument (*instrument II*).